PSFC/JA-04-44

Transport-Driven Scrape-off Layer Flows and the X-Point Dependence of the L-H Power Threshold in Alcator C-Mod

B.LaBombard, J.E. Rice, A.E. Hubbard, J.W. Hughes, M. Greenwald, R.S. Granetz, J.H. Irby, Y. Lin, B. Lipschultz, E.S. Marmar, K. Marr, D. Mossessian, R. Parker, W. Rowan†, N. Smick, J.A. Snipes, J.L. Terry, S.M. Wolfe, S.J. Wukitch and the Alcator C-Mod Team

16 November 2004

Massachusetts Institute of Technology, Plasma Science and Fusion Center
Cambridge, MA 02139 USA

†University of Texas, Fusion Research Center, Austin, TX 78712

This work was supported by the U.S. Department of Energy, Cooperative Grant No. DE-FC02-99ER54512. Reproduction, translation, publication, use and disposal, in whole or in part, by or for the United States government is permitted.

Submitted for publication to *Physics of Plasma.*

Transport-driven scrape-off layer flows and the x-point dependence of the L-H power threshold in Alcator C-Mod

B. LaBombard*, J.E. Rice, A.E. Hubbard, J.W. Hughes, M. Greenwald,
R.S. Granetz, J.H. Irby, Y. Lin, B. Lipschultz, E.S. Marmar, K. Marr, D. Mossessian,
R. Parker, W. Rowan†, N. Smick, J.A. Snipes, J.L. Terry, S.M. Wolfe, S.J. Wukitch
and the Alcator C-Mod Team

Massachusetts Institute of Technology, Plasma Science and Fusion Center
175 Albany St., Cambridge, MA 02139 USA

†*University of Texas, Fusion Research Center, Austin, TX 78712*

Factor of ~2 higher power thresholds for low- to high-confinement mode transitions (L-H) with unfavorable x-point topologies in Alcator C-Mod [Phys. Plasmas **1**, 1511 (1994)] are linked to flow boundary conditions imposed by the scrape-off layer (SOL). Ballooning-like transport drives flow along magnetic field lines from low- to high-field regions with toroidal direction dependent on upper/lower x-point balance; the toroidal rotation of the confined plasma responds, exhibiting a strong counter-current rotation when $Bx\nabla B$ points away from the x-point. Increased auxiliary heating power (rf, no momentum input) leads to an L-H transition at approximately twice the edge electron pressure gradient when $Bx\nabla B$ points away. As gradients rise prior to the transition, toroidal rotation ramps toward the co-current direction; the H-mode is seen when the counter-current rotation imposed by the SOL flow becomes compensated. Remarkably, L-H thresholds in lower-limited discharges are identical to lower x-point discharges; SOL flows are also found similar, suggesting a connection.

PACS: 52.30.-q, 52.25.Fi, 52.25.Gj, 52.40.Hf, 52.55.Fa, 52.70.Ds, 52.70.Nc

* Tel.: 1-617-253-7264, Fax: 1-617-253-0627: e-mail: labombard@psfc.mit.edu

I. INTRODUCTION

H-mode energy confinement [1] is essential for optimizing tokamak performance; reactor concepts typically project to ignition conditions based on achieving this regime. It is therefore important to understand the physical mechanisms that control access to H-modes in a tokamak. A leading explanation for the transition from low to high confinement mode (L-H) involves ExB velocity shear[2-6], resulting in a bifurcation in plasma transport characteristics near the vicinity of the separatrix. While this physics may explain the existence of an L-H power threshold, no compelling explanation has been advanced to account for the higher input powers required when $Bx\nabla B$ points away from rather than toward the active x-point [7]. Edge conditions associated with the threshold (e.g., critical temperature or its gradient) are also found to change substantially; a factor of ~2 increase in edge electron temperature accompanies a factor of ~2 higher power threshold in Alcator C-Mod [8] and elsewhere [9]. Most notably, when magnetic topology alone is changed (at fixed power levels), no obvious differences in the L-mode edge profiles are evident (e.g. [10]) while some unexplained changes in edge velocity shear have been seen [11], offering few clues about the physics that causes differences in H-mode accessibility. Nevertheless, the pervasive sensitivity of the L-H power threshold to x-point topology seen in experiments suggests that there must be a correspondingly robust explanation – something that perhaps involves the time-averaged 'equilibrium' plasma state at a fundamental level, an equilibrium that is necessarily constrained by the underlying micro-turbulence that regulates transport.

In this paper, we summarize recent experimental results from Alcator C-Mod [12] indicating that L-mode plasma equilibria are indeed fundamentally different in upper versus

lower x-point topologies, despite superficial similarities in plasma profiles. Key experimental observations are: strong plasma flows in the scrape-off layer (SOL), a dependence of the flow on the magnetic topology, and the coupling of the flow momentum across the separatrix (i.e., a flow 'boundary condition') to produce a topology-dependent toroidal rotation of the confined plasma. The origin of the SOL flow is connected to the ballooning-like nature of edge plasma micro-turbulence. Consistent with the toroidal rotation of the confined plasma, electric potentials and radial electric fields in the SOL are observed to also be topology-dependent: larger electric fields and field gradients are detected when $Bx\nabla B$ is directed toward the x-point with all other external control parameters being the same. Thus, the experimental observations suggest that differences in equilibrium ExB flow shear may be responsible for the differences in L-H power thresholds. It should be emphasized that *direct* experimental evidence of equilibrium flow-shear (topology-dependent or otherwise) influencing turbulence and transport in these discharges has yet to be obtained. Nevertheless, the aggregate of experimental observations form a compelling story; the sensitivity of the L-H power threshold to x-point topology may ultimately be understood in terms of the flow boundary conditions imposed by the scrape-off layer.

The paper is organized as follows: plasma discharge conditions, magnetic topologies and flow diagnostics are discussed briefly in section II. Experimental evidence for ballooning-like transport causing strong flows along field lines in the SOL (i.e., *transport-driven* flows) is presented in section III. A connection is made between SOL flows and toroidal plasma rotation by examining their dependences on x-point topology. Section IV summarizes recent experimental observations that link the behavior of SOL flows to the differences seen in L-H power thresholds. In addition, new information from limiter-defined flux surface topologies is

presented, including discharges that were limited on the inner wall near the midplane and on an inner wall surface near the lower divertor, as was recently reported in [13]. Remarkably, L-H thresholds for lower-limited discharges are found identical to lower x-point discharges. The sensitivity of the L-H power threshold to magnetic topology is examined in terms of this new insight; the degree to which the magnetic configuration allows transport-driven co-current flows to exist in the high-field side SOL is suggested as a controlling element. Principal findings are summarized in section V.

II. EXPERIMENTAL ARRANGEMENT

Information on Alcator C-Mod's overall design and operational characteristics can be found in reference [14]. Results reported in this paper were obtained in deuterium discharges with toroidal magnetic field strength (B_T) of 5.4 tesla, plasma currents (I_p) of 0.8 MA (excepting one inner-wall limited discharge with I_p=1.0 MA), B_T and I_p in the same direction and $B \times \nabla B$ pointing toward the bottom of the device. Plasma densities during the L-mode phase were programmed to be within one of two line-averaged density groups: a low-density range, 0.9 < $\overline{n}_e$ < 1.2 x10^{20} m^{-3} and a mid-density range, 1.3 < $\overline{n}_e$ < 1.8 x10^{20} m^{-3}. Results from an inner-wall limited plasma with $\overline{n}_e$ = 2.0 x10^{20} m^{-3} are also reported.

Experiments were performed using six different magnetic configurations. The first-wall geometry and magnetic equilibria from representative discharges (computed from the EFIT plasma equilibrium code [15]) are shown in Fig. 1. Figure 1 also defines acronyms to indicate the last closed flux surface (LCFS) topologies: upper single null (USN), lower single null (LSN), double null (DN), inner divertor nose-grazing (ING), inner divertor nose-limited (INL), and

inner wall limited (IWL). Note that in ING and INL discharges, the LCFS interacts with a section of the inner wall at the entrance to the lower divertor (i.e., the 'inner divertor nose'). In these equilibria, flux surfaces pass without obstruction through the gap (~2 cm) between the LCFS and the inner wall at the midplane. In contrast, the midplane gap is zero in IWL discharges (by definition). Some LSN discharges were run with reduced inner midplane gap; these are designated as reduced-gap LSN discharges (RGLSN).

Figure 1 shows the measurement locations of four diagnostics used to infer plasma flow. Three scanning probes are employed [12]; two scan along a major radius through the high and low-field regions of the SOL ('inner' and 'outer' scanning probes) and one scans vertically from the bottom of the vessel ('vertical' probe). These probes are configured as Langmuir-Mach probes and infer cross-field profiles of plasma density (n), electron temperature (T_e) and plasma flow along magnetic field lines in terms of a parallel Mach number, $M_{//}$. Fluctuations in ion saturation current (bandwidth of 5 - 500 kHz) are also recorded.

Central plasma rotation velocities are inferred from the toroidal motion of Ar^{17+} ions. Doppler shifts of the corresponding Ly_α doublet are viewed along a toroidal line of sight tangent to the plasma center, using a fixed von Hamos type crystal x-ray spectrometer [16]. Trace amounts of argon are injected early in the discharge to facilitate the measurement. On the basis of neoclassical theory [17], the difference between Ar^{17+} and majority ion toroidal rotation velocities is estimated to be small relative to the characteristic velocities (and most importantly, the *changes* in velocities) that are reported here. An independent inference of toroidal plasma rotation through sawtooth oscillations [18,19] verifies that the Ar^{17+} ions are close to the toroidal rotation of the plasma background.

Ion-cyclotron range-of-frequency (ICRF) heating power is applied to L-mode 'target' plasmas using either a slow ramp-up in power to determine the L-H threshold or a fixed power level near threshold to study the L-H transition in detail. This power is from 2 two-strap antennas (80 MHz, 0 - π phasing) and one four-strap antenna (78 MHz, 0 - π - 0 - π phasing), employing a hydrogen minority heating scenario. It is important to note that this heating method imparts no direct momentum input to the plasma.

III. TRANSPORT-DRIVEN SOL FLOWS AND PLASMA ROTATION

A. SOL profiles and flows

Scanning Langmuir-Mach probe measurements have uncovered clear evidence of strong ballooning-like transport and associated transport-driven plasma flow along field lines in the inner SOL (i.e., the high-field side SOL). A compilation of cross-field plasma profiles, including flow measurements, in the inner and outer SOL regions for USN, DN and LSN equilibria is shown in Fig. 2. The curves represent averages of 33 probe scans in L-mode discharges with density range $0.9 < \overline{n}_e < 1.2 \times 10^{20}$ m^{-3}. Vertical bars indicate ±1 standard deviation, computed from the sample variance.

In single null discharges (USN, LSN), electron pressure profiles map along field lines to within about a factor of ~2. However, in DN discharges, plasma in the inner SOL practically disappears! The pressure e-folding length in this region is reduced by a factor of ~4, even though the profiles in the outer SOL remain essentially unchanged. The behavior of plasma fluctuations (quantified here as the rms fluctuation in ion saturation current divided by the mean value) suggests an explanation: turbulence and cross-field transport have a strong ballooning-like character; normalized plasma fluctuations near the separatrix are a factor of ~3 or more lower in

the inner SOL, independent of topology. Apparently, plasma 'fills-in' the inner SOL in single null discharges not by cross field transport but by plasma flow along magnetic field lines. The plasma flow data in the lower left panel of Fig. 2 independently support this explanation. Remarkably fast parallel plasma flows are detected on the inner SOL. (The toroidal projection of this parallel velocity is shown. For comparison, a typical plasma sound speed is ~50 km s^{-1}.) The direction of the flow is found to depend on magnetic topology – counter-current for USN, co-current in LSN and nearly stagnant in DN – precisely the response expected for *transport-driven* flows, i.e., flows arising from ballooning-like transport. The direction of the flow (co- or counter-current) depends on how field lines connect between the low and high-field SOL regions, which depends on the x-point topology. In earlier experiments where the upper/lower x-point balance was systematically change from LSN to USN, the location of a steep gradient 'breakpoint' in the inner SOL profiles, as measured both by the inner scanning probe and by D_α emission near the inner wall, was found to track with the secondary separatrix [20], i.e., the location in the profile where field lines no longer map between high and low-field SOL regions.

Note that flows in the outer SOL (lower right panel of Fig. 2) are relatively weak and persistently co-current directed under these discharge conditions (although the magnitude appears affected by topology). One might expect the transport-driven component of the flow to be nearly stagnant at this location since it may correspond to the top-bottom symmetry point of a ballooning-like drive. Further analysis, including discharges with reversed directions of B_T and I_p, indicate that a large fraction of the total flow can indeed be explained in terms of other effects, e.g., a combination of pure toroidal rotation and Pfirsch-Schlüter ion flows [12].

B. Transport-driven SOL flows

A simple technique for extracting just the transport-driven component of the flow is to map USN/LSN measurements onto appropriately defined flux-tube coordinates and take the average. Flow contributions from toroidal rotation, Pfirsch-Schlüter ion flows, or systematic offsets in the inferred Mach number change sign in this mapping process and therefore cancel – if these contributions are the same in matched USN/LSN discharges. A representative result from this 'flux-tube mapping' procedure is shown in Fig. 3. The definition of the flux tube coordinate, *S*, is shown at the bottom. Data points from the inner, outer, and vertical scanning probes are included (ρ = 4 mm). Triangles (color-coded according to USN/LSN) represent average values while the vertical bars indicate ±1 standard deviation. The data are taken from the same set of discharges as in Fig. 2.

A persistent trend of parallel plasma flow from outer to inner SOL is evident in Fig. 3. Offsets about this trend that depend on x-point location are also seen (presumably caused by some combination of toroidal rotation, Pfirsch-Schlüter ion flows and systematic Mach-probe offsets). The electron pressures on the inner SOL (nT_e) tend to be lower than on the outer SOL. These data are again consistent with the notion that plasma is driven from outer to inner SOL regions as a result of pressure variation along field lines.

In the bottom panel of Fig. 3, the quantity $nT_e(1 + M_{//}^2 / 2)$ is shown; it represents the sum of the plasma's thermal and flow energy densities. In a Maxwellian plasma with $T_i = T_e$ and with no density variation along field lines (a situation approximating the experimentally observed conditions), this quantity will be conserved if there is no momentum source (or sink) in the flux tube. Possible momentum sources include turbulence-induced Reynolds stress or

interaction with neutrals. However, within the experimental uncertainty, this quantity is conserved. Therefore, the transport-driven flow appears to be a simple, free-streaming plasma flow; no exotic flow drive mechanism other than ballooning-like cross-field transport need be postulated.

Note that a steady-state plasma flow loop is implied, as illustrated in the bottom of Fig. 3: excess plasma enters flux tubes near the outer SOL; a large fraction of this flows along field lines to the inner SOL and presumably neutralizes at or near the inner divertor surface (via surface or volume recombination). In order to close the loop, neutrals likely ionize inside the separatrix near the inner divertor leg; the resulting ions are free to over-populate flux tubes in the outer SOL once again. Such a large-scale plasma convection pattern is consistent with flow observations from a number of other experiments, including: the x-point dependence of impurity 'plumes' at the inner midplane of Alcator C-Mod [21], the persistent parallel plasma flow from outer to inner divertor measured near the top of JET [22] and associated with the build-up of carbon 'flakes' on the inner divertor [23], and more recently, the migration of ^{13}C towards the inner divertor in response to $^{13}CH_4$ injected at the top of the torus in JET [24] and in DIII-D [25].

C. Toroidal rotation boundary condition

Recent measurements of toroidal momentum transport in Alcator C-Mod clearly illustrate the role that the edge plasma plays in defining the rotation boundary condition for the core [16]. Immediately after an L-H transition, a prompt increase in co-current rotation is seen, starting near the edge and propagating into the plasma center over timescales on the order of the energy confinement time. Therefore, it is interesting to consider the boundary condition that the

transport-driven SOL flow pattern (illustrated in Fig. 3) presents to the confined plasma; the volume averaged flow has a non-zero toroidal velocity – co-current directed for LSN and counter-current directed for USN. Does the confined plasma respond in any significant way to this topology-dependent boundary condition? Figure 4 shows plasma flow measurements from a series of matched discharges ($1.3 < \overline{n}_e < 1.8$ x10^{20} m^{-3}) in which the balance between upper and lower x-point was systematically varied. Toroidal projections of flow velocities measured by the inner and outer probes near the separatrix (ρ = 2 and 1 mm) are shown in the top two panels. The bottom panel shows corresponding measurements of toroidal velocity at the plasma center. A clear correlation is seen among all three; flow velocities systematically increment towards the counter-current direction in the sequence LSN, DN, USN. The largest change in flow velocity is seen on the inner SOL – consistent with the idea that this flow is responsible for the toroidal velocity changes measured elsewhere. The velocities also display a remarkable sensitivity to magnetic topology: a ~5 mm shift in the x-point balance is sufficient to completely reverse the flows. This size scale is comparable to the pressure gradient scale lengths near the separatrix (Fig. 2) – an expected result if in/out pressure asymmetries on open field lines are the principal drive mechanism.

We also find that topology-induced velocity changes in the outer SOL and at the center vary with discharge density, with a trend of becoming weaker at lower density [12]. However, under all conditions studied, the velocity change in the inner SOL is largest, maintaining the values shown in Fig. 4.

The apparent momentum coupling between SOL and confined plasma regions may be likened to the physics of a waterwheel: plasma (~water) is 'injected' into the outer SOL (~the

top of the wheel) and flows fastest and over the longest distance in the direction of the inner divertor (~falls down one side of the wheel more than the other); the confined plasma (~wheel) rotates in the direction of least resistance – toroidally. However, unlike the waterwheel analogy, plasma is 'injected' into the SOL at the toroidal velocity of the confined plasma. Therefore, the SOL plasma should exhibit an increase or decrease in toroidal rotation that mimics the confined plasma, if the above picture is correct. Moreover, any change in toroidal rotation of the SOL, ΔV_ϕ, requires a corresponding change in the SOL's radial electric field, $\Delta E_r = \Delta V_\phi B_\theta$ (see illustration at the bottom of Fig. 5).

To test these ideas, we have assembled plasma potential profiles from the scanning probe data and investigated their sensitivities to x-point topology. The potential profiles shown in Fig. 5 correspond to the discharges of Fig. 2 and were computed using an estimate of the plasma-probe sheath potential drop from probe theory. (A word of caution is appropriate here. Plasma potentials inferred by this method should be considered as providing only qualitative information since the resultant E_r have been found inconsistent with other methods [12]. Nevertheless, a *change* in potential with topology should be an indicator of the *change* in true plasma potential, when all other plasma conditions remain the same.) A trend of increasing plasma potential near the separatrix in the sequence USN, DN, LSN is evident in Fig. 5; E_r, averaged over the SOL, roughly increases by a total of ~5kV m^{-1}; this corresponds to a toroidal rotation velocity increase in the co-current direction of ΔV_ϕ ~8 km s^{-1} – a value consistent in sign and magnitude to the measured change in toroidal velocity in the outer SOL (see Fig. 2). It also appears that the curvature of the potential profile near the separatrix (~gradient in E_r, or equivalently, velocity shear) tends to be largest in LSN, although uncertainties in this quantity prevent any firm

conclusion. Nevertheless, one would expect the velocity shear to be roughly proportional to the magnitude of the toroidal rotation at the separatrix since the velocity is ~0 at the wall while the SOL width remains roughly constant. Recent results from gas-puff imaging of SOL turbulence are consistent with an increase in E_r in going from USN and LSN [26]; plasma fluctuations are found to propagate more strongly in the ion diamagnetic direction for LSN.

IV. L-H TRANSITIONS AND MAGNETIC TOPOLOGY

A. Comparison of LSN, DN and USN discharges

A number of key observations pertaining to the x-point dependence of the L-H transition in Alcator C-Mod can be summarized with the help of Fig. 6. Data traces are overlaid from three plasmas (LSN, DN, USN) with otherwise identical initial conditions. Following a steady-state ohmic phase, ICRF heating power is applied at levels close to the threshold (0.9, 1.6, 2.9 MW) to induce an L-H transition later in time. Note that this heating method imparts no momentum to the plasma. During the ohmic phases, electron temperatures at the 95% flux surface ($\psi = 0.95$), as inferred from Thomson scattering (TS) and electron cyclotron emission (ECE), as well as edge electron pressure gradients ($0.95 < \psi < 1$) are essentially identical. However, the toroidal rotation velocity at the plasma center is markedly different – this observation can now be understood in terms of topology-dependent flow boundary conditions imposed by the SOL flows (Fig. 4). In response to the application of ICRF heating power, another interesting behavior occurs. The plasmas do not immediately make the transition into H-mode. Instead, a slow increase in edge temperature and pressure gradient occurs – most noticeably for the USN case, which has higher input power. Associated with the pressure gradient increase is a gradual shift of core toroidal rotation toward the co-current direction, again largest in the highest input power

case. Just prior to the L-H transition, edge electron temperatures and pressure gradients are a factor of ~2 higher in USN versus LSN, similar to differences seen with forward versus reversed magnetic field and fixed x-point location [8]. The one feature that appears constant at the L-H transition is the toroidal rotation velocity; it has roughly the same value at transition, independent of topology. Such an association between toroidal rotation level and the attainment of an L-H transition has been noted previously in comparing the time evolution of otherwise identical DN and USN discharges [16].

Apparently, a key component of the L-H threshold puzzle is the ramp-up behavior of the plasma rotation during the L-mode phase of USN discharges. Plasma flows (rotation) measured by Mach probes near the separatrix are found to exhibit a similar behavior, tracking proportionally the co-current increase in central rotation with increased input power (see Fig. 20 of Ref. [12]). Thus, the central plasma rotation measurement may be considered a rough measure of the edge plasma rotation during the L-mode phase and, by inference, be related to the radial electric fields there (allowing for offsets that may include rotation profile effects). Taken together, the following picture emerges: topology-dependent SOL flows set a favorable (LSN) or unfavorable (USN) toroidal rotation boundary condition on the confined plasma. The increased input power (~higher pressure gradients) in USN shift the toroidal rotation in the direction of the plasma current. The L-H transition occurs in USN when the unfavorable SOL flow boundary condition becomes compensated. This compensation requires higher input powers. While the physics of the L-H transition presumably involves velocity shear at the edge (a quantity that is not presently measured in these experiments), the relative magnitude of the toroidal rotation at the edge appears to be acting as an effective proxy for this quantity.

The principal mechanism that causes the co-current rotation shift with increased plasma pressures has not yet been identified. However, a similar effect has been observed during the H-mode phase of ohmic or ICRF heated plasmas [27]; the level of central plasma rotation is found to correlate with plasma stored energy (~plasma pressure gradient). A number of theoretical explanations has been advanced for this behavior, including plasma turbulence [28,29] and sub-neoclassical transport [30].

B. Comparison of LSN, ING and INL discharges

It is often thought that in order to achieve H-modes at low input power levels, a magnetic separatrix is a necessary ingredient; when the LCFS is defined by a limiter surface, L-H power thresholds are usually observed to be higher. This operational experience has focused attention on the physics of the x-point region itself (e.g., magnetic shear, ion orbit loss) and/or the physics associated with the proximity of the LCFS to the first-wall (e.g., neutral interaction, impurity generation) as being controlling elements. However, contrary to these expectations, we find the L-H power threshold to be virtually identical in lower-limited versus lower x-point discharges in Alcator C-Mod.

Figure 7 shows a comparison of signals from three well-matched discharges with x-point and limiter-defined LCFS topologies: LSN, ING, and INL. As can been seen by the overlaid waveforms of line-averaged density and ICRF power, no significant difference in the L-H power threshold is detected; it does not matter if the lower x-point is centered above the divertor (LSN), on the inner divertor nose (ING) or buried inside the vacuum vessel wall (INL). However, the D_α photodiode signal level is different. This is because the overall level and spatial distribution of ionization and recombination in the lower divertor region changes with magnetic

configuration.

So what is the common element that makes the L-H threshold identical in these discharges? Although plasma physics associated the x-point itself is by definition absent in INL discharges, one could argue that the x-point region still plays a role; a significant spatial modulation in the poloidal field at the LCFS does persist in all three cases. Additionally, the connection lengths along magnetic field lines to material surfaces are similar, potentially allowing electron temperatures near the separatrix to remain the same even in the INL case. However, the magnetic equilibria exhibit another potentially important commonality – they all enforce the same SOL flow pattern!

Figure 8 shows a compilation of cross-field profiles for USN, LSN, ING and INL equilibria, in the same format as Fig. 2. Data from 49 probe scans are included with density range, $0.8 < \overline{n}_e < 1.2 \times 10^{20}$ m^{-3}. The USN/LSN profiles were assembled from different discharges than those of Fig. 2, yet they essentially overlay with the profiles in that figure. These profiles serve as a reference for the ING/INL data. Electron pressure profiles in ING/INL are found to be similar to USN/LSN discharges, except for increased pressures and flatter profiles far into the SOL. In/out asymmetries in plasma fluctuations are virtually unchanged and similarly strong. The most interesting result is the behavior of the SOL flows: inner SOL flows in ING/INL discharges are found to be identical to those of LSN discharges – co-current directed in the SOL. Outer SOL flows in ING/INL discharges are also similar to those of LSN discharges (and USN discharges, since topology-induced differences are small at this location). Toroidal rotation velocities measured at the plasma center (not shown) in ING/INL discharges are found to be the same as in LSN, within experimental uncertainties.

If SOL flow boundary conditions are taken to be an overriding factor in controlling the L-H power threshold, then the puzzle presented by Fig. 7 can be resolved. Although the separation distance between the LCFS and wall changed from ~15 mm to zero in going from LSN to INL, the poloidal locations of wall contact (ING, INL) and x-point location (LSN) were similar; consequently, the transport-driven SOL flow patterns were unchanged. This insight may help us understand L-H power threshold observations in inner-wall limited discharges (IWL). Similar to other experiments, we find the L-H power threshold for IWL to be greater than a factor of ~2 higher than in LSN – exceeding the USN L-H threshold. In the past, we had attributed this high threshold to the lack of (unknown) x-point physics, to lowered plasma temperatures at the separatrix due do shorter magnetic connection lengths, and/or the poor screening of impurities from the inner wall. These elements may indeed be important. However, another possible contributor may be the lack of a favorable SOL flow pattern. The top-bottom symmetry of the SOL in IWL should cause the toroidal-projection of transport-driven parallel flows to average to zero.

Finally it should be noted that IWL discharges are typically run in C-Mod with a lower x-point close to the LCFS (see typical IWL equilibrium in Fig. 1). IWL discharges are often formed by 'bumping' the separatrix against the inner wall. Therefore, if poloidal field modulation at the LCFS is playing any beneficial role, it is dwarfed by other (negative) effects in these IWL discharges.

C. Summary of L-H power thresholds versus topology

Building on the idea that LCFS topology affects the L-H power threshold through control of SOL flows, it is possible to unify the threshold observations, as shown in Fig. 9. These data

were taken from 7 different magnetic configurations, as indicated. The vertical axis is the total input power at L-H transition normalized to a scaling law for L-H power thresholds, P_L, compiled from the International H-mode Threshold Database [31],

$$P_L \equiv 0.054\,\bar{n}_e^{0.49} B_T^{0.85} S^{0.84} \quad . \qquad (1)$$

P_L has units of MW, $\bar{n}_e$ is the line-averaged density (10^{20}m^{-3}), B_T is the toroidal field on axis (tesla) and S is the plasma surface area (m^2). The scaling law applies to single-null configurations with favorable x-point location (i.e., LSN with $B x \nabla B$ pointing down) and to discharges above an empirically observed 'low density limit.' To satisfy the latter criterion, only discharges with $\bar{n}_e > 1.3\text{x}10^{20}$ m^{-3} are included in Fig. 9, since LSN discharges under this density were found to depart systematically from the empirical law, having a higher threshold power. Each discharge is assigned a position on the horizontal axis in Fig. 9 based on the smaller of two quantities: (i) the distance between primary and secondary separatrices mapped to outer midplane or (ii) the gap between the LCFS and the inner wall at the midplane. This value, Δ, is written as a negative number for discharges with a lower x-point or a lower limiter defined LCFS. Thus, Δ parameterizes both the direction of the transport-driven flows on the inner SOL (negative = co-current) and the width of the inner SOL available for these flows.

Figure 9 captures the essence of the observed threshold dependences in Alcator C-Mod and hints at possible explanations: INL, ING and LSN discharges, which have large negative Δ and therefore favorable SOL flows, have the same power thresholds. As Δ approaches zero (starting near -5 mm), the power threshold begins to rise – this is seen in near-balanced DN discharges and 'reduced-gap' LSN discharges (RGLSN). As shown in Fig. 4, this is precisely the spatial scale at which the transport-driven SOL flows are affected by topology changes. As Δ

increases through zero, a further increase in power threshold is seen, leveling out when Δ increases above +5 mm. These USN discharges have transport-driven SOL flows in the unfavorable direction. IWL discharges have the highest normalized thresholds. Part of the reason may be connected to the lack of rotation drive from SOL flows in this top-bottom symmetric geometry. However, the IWL threshold is significantly above that of DN, pointing towards other effects. In addition, we have found H-modes in the IWL configuration to be short-lived transient phenomena, further suggesting compound influences.

V. SUMMARY

Recent experiments on Alcator C-Mod have uncovered a novel explanation for the x-point sensitivity of the L-H power threshold, involving boundary conditions imposed by topology-dependent *transport-driven* flows in the SOL.

A strong ballooning-like cross-field transport asymmetry is identified as causing near-sonic flows in the high-field SOL (hence their designation as transport-driven flows). As a result, the SOL possesses a volume-averaged toroidal velocity component that depends on x-point location, being co-current directed in lower x-point discharges with $B x \nabla B$ pointing down. The flows are seen to impose boundary conditions on the confined plasma; toroidal rotation near the separatrix and in the plasma center are found to track with changes in upper/lower x-point flux balance; corresponding changes in radial electric fields in the SOL are consistent with changes in toroidal rotation.

The power level to achieve an L-H transition and the toroidal rotation of the confined plasma are found to be connected. In upper x-point discharges, the SOL flows impose a counter-current offset to the toroidal rotation. However, upon application of ICRF heating (no

momentum input), the toroidal rotation of the plasma shifts towards the co-current direction as pressure gradients in the edge increase. The L-H transition is observed when the counter-current rotation offset becomes compensated, requiring a factor of ~2 higher input power with correspondingly larger edge pressure gradients.

L-H thresholds in lower x-point and lower-limited discharges are found to be identical. The corresponding SOL flow patterns are also found identical, consistent with the notion that SOL flows play a controlling role in L-H threshold physics. The sensitivity of the L-H threshold to last closed flux surface topology can be viewed more generally in terms of the direction of the transport-driven flows on the inner SOL (co- or counter-current) and the width of the inner SOL available for these flows to encircle the confined plasma.

Acknowledgements

Alcator C-Mod's contributions to fusion energy science are made possible by the excellent engineers, technical staff, students, and scientists on the Alcator team. This work is supported by U.S. Department of Energy Coop. Agreement DE-FC02-99ER54512.

References

[1] F. Wagner, G. Becker, K. Behringer et al., Phys. Rev. Lett. 49, 1408 (1982).
[2] H. Biglari, P.H. Diamond, and P.W. Terry, Phys. Fluids 2, 1 (1990).
[3] R.J. Groebner, K.H. Burrell, and R.P. Seraydarian, Phys. Rev. Lett. 64, 3015 (1990).
[4] K.H. Burrell, Phys. Plasmas 4, 1499 (1997).
[5] J.W. Connor and H.R. Wilson, Plasma Phys. Control. Fusion 42, 1 (2000).
[6] P.W. Terry, Rev. Mod. Phys. 72, 109 (2000).
[7] F. Ryter and H Mode Database Working Group, Nucl. Fusion 36, 1217 (1996).
[8] A. E. Hubbard, R. L. Boivin, J. F. Drake, M. Greenwald, Y. In, J. H. Irby, B. N. Rogers, and J. A. Snipes, Plasma Phys. Control. Fusion 40, 689 (1998).
[9] F. Ryter, W. Suttrop, B. Brusehaber et al., Plasma Phys. Control. Fusion 40, 725 (1998).
[10] T.N. Carlstrom, K.H. Burrell, R.J. Groebner, A.W. Leonard, T.H. Osborne, and D.M. Thomas, Nucl. Fusion 39, 1941 (1999).

[11] T. N. Carlstrom, R. J. Groebner, C. Fenzi, G. R. McKee, R. A. Moyer, and T. L. Rhodes, Plasma Phys. Control. Fusion 44, A333 (2002).
[12] B. LaBombard, J. E. Rice, A. E. Hubbard et al., Nucl. Fusion 44, 1047 (2004).
[13] A. E. Hubbard, B. LaBombard, J. E. Rice et al., "Dependence of the C-Mod L-H Threshold on Magnetic Configuration and Relation to Scrape-off-layer Flows," in *Controlled Fusion and Plasma Physics* (European Physical Society, Geneva (2004), London, UK, 2004), Vol. 28B.
[14] I. H. Hutchinson, R. Boivin, F. Bombarda et al., Phys. Plasmas 1, 1511 (1994).
[15] L. L. Lao, H. St. John, R. D. Stambaugh, A.G. Kellman, W. Pfeiffer, and Nucl. Fusion 25 (1985) 1611, Nucl. Fusion 25, 1611 (1985).
[16] J. E. Rice, W. D. Lee, E. S. Marmar et al., Nucl. Fusion 44, 379 (2004).
[17] Y.B. Kim, P.H. Diamond, and R.J. Groebner, Phys. Fluids 3, 2050 (1991).
[18] J.E. Rice, M. Greenwald, I.H. Hutchinson, E.S. Marmar, Y. Takase, S.T. Wolfe, and F. Bombarda, Nucl. Fusion 38, 75 (1998).
[19] I.H. Hutchinson, J.E. Rice, R.S. Granetz, and J.A. Snipes, Phys. Rev. Lett. 84, 3330 (2000).
[20] C J Boswell, J L Terry, B LaBombard, B Lipschultz, and C S Pitcher, Plasma Phys. Control. Fusion 46, 1247 (2004).
[21] D. Jablonski, B. LaBombard, G. M. McCracken, S. Lisgo, B. Lipschultz, I. H. Hutchinson, J. Terry, and P. C. Stangeby, J. Nucl. Mater. 241-243, 782 (1997).
[22] S. K. Erents, A. V. Chankin, G. F. Matthews, and P. C. Stangeby, Plasma Phys. Control. Fusion 42, 905 (2000).
[23] J.P. Coad, N. Bekris, J.D. Elder, S.K. Erents, D.E. Hole, K.D. Lawson, G.F. Matthews, R.-D. Penzhorn, and P.C. Stangeby, J. Nucl. Mater. 290-293, 224 (2001).
[24] J. Likonen, S. Lehto, J. P. Coad, T. Renvall, T. Sajavaara, T. Ahlgren, D. E. Hole, G. F. Matthews, and J. Keinonen, Fusion Engineering and Design 66-68, 219 (2003).
[25] S.L. Allen, A.G. McLean, W. R. Wampler et al., submitted to J. Nucl. Mater. (2004).
[26] J.L. Terry, S.J. Zweben, O. Grulke, M.J. Greenwald, and B. LaBombard, to be published in J. Nucl. Mater. (2004).
[27] J.E. Rice, R.L. Boivin, P.T. Bonoli et al., Nucl. Fusion 41, 277 (2001).
[28] K.C. Shaing, Phys. Rev. Lett. 86, 640 (2001).
[29] B. Coppi, Nucl. Fusion 42, 1 (2002).
[30] A.L. Rogister, J.E. Rice, A. Nicolai, A. Ince-Cushman, and S. Gangadhara, Nucl. Fusion 42, 1144 (2002).
[31] J.A. Snipes, Plasma Phys. Control. Fusion 42, 299 (2000).

Figure captions

Figure 1. X-point and limiter-defined magnetic configurations in Alcator C-Mod. Scanning Langmuir-Mach probes infer plasma profiles and parallel flows at three locations in the scrape-off layer, including the high-field side (Inner Scanning Probe). Central plasma rotation is inferred from x-ray spectroscopy, viewing the Doppler-shifts of Ly_α emission from central Ar^{17+} ions.

Figure 2. Scrape-off layer profile and flow data obtained from the inner and outer scanning probes. The flux surface coordinate, ρ, is the distance into the SOL, mapped to the outer midplane. Shaded regions indicate where field lines may contact limiter surfaces. Positive velocities correspond to flow in the co-current direction.

Figure 3. Probe data mapped onto a flux tube coordinate system (top panels) and implied transport-driven plasma flow pattern (bottom). Straight lines connecting between symbols are included to guide the eye. Positive Mach number corresponds to flow in the direction of S.

Figure 4. Toroidal projection of parallel flows measured near the separatrix by probes (top two panels) and toroidal rotation velocity measured at the plasma center (bottom panel). Positive velocity is in the direction of plasma current. The distance between primary and secondary separatrix surfaces (mapped to the outer midplane) is used to parameterize the upper/lower x-point balance.

Figure 5. Plasma potential profiles in LSN/DN/USN discharges estimated from scanning probes (top panels) and the expected changes in SOL radial electric fields (bottom).

Figure 6. Time histories of thee discharges exhibiting L-H transitions near power threshold. The time axis is offset, placing zero at the time of L-H transition. Positive velocity corresponds to toroidal rotation in the co-current direction (bottom panel).

Figure 7. Time histories of LSN, ING and INL discharges exhibiting L-H transitions. Dashed lines indicate times of L-H transitions.

Figure 8. SOL profiles for USN, LSN, ING and INL configurations. Shaded regions indicate where field lines may connect to limiter surfaces other than the inner divertor 'nose'. Positive velocities correspond to flow in the co-current direction.

Figure 9. L-H power thresholds observed for 7 different x-point and limiter-defined magnetic configurations, normalized by a scaling law for LSN power thresholds [Eq. (1)]. The parameter, Δ, corresponds to the smaller of (i) the distance between primary and secondary separatrix surfaces (mapped to outer midplane) or (ii) the distance from the LCFS to the inner wall midplane, multiplied by minus one when a lower x-point or a lower limiter surface defines the LCFS.

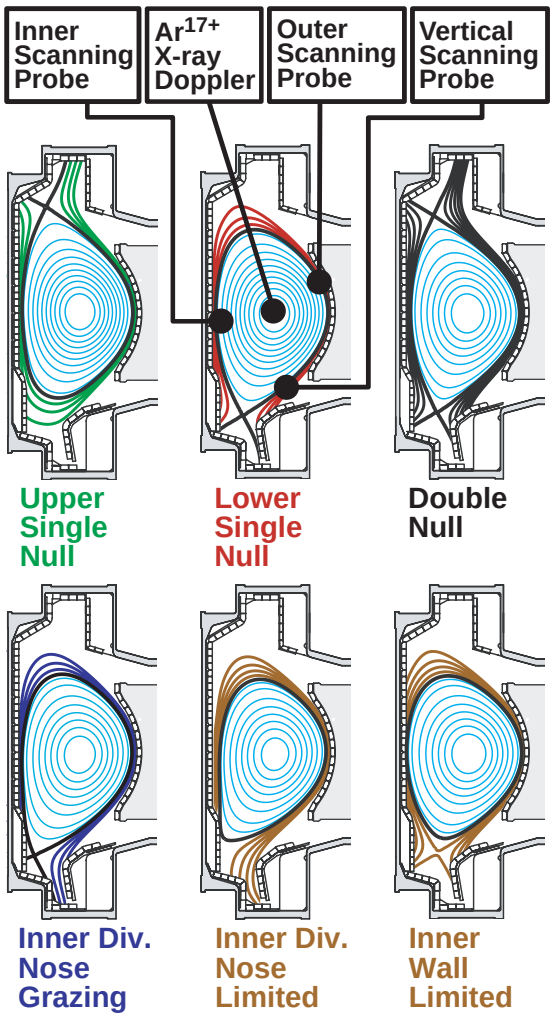

Figure 1. X-point and limiter-defined magnetic configurations in Alcator C-Mod. Scanning Langmuir-Mach probes infer plasma profiles and parallel flows at three locations in the scrape-off layer, including the high-field side (Inner Scanning Probe). Central plasma rotation is inferred from x-ray spectroscopy, viewing the Doppler-shifts of Ly_α emission from central Ar^{17+} ions.

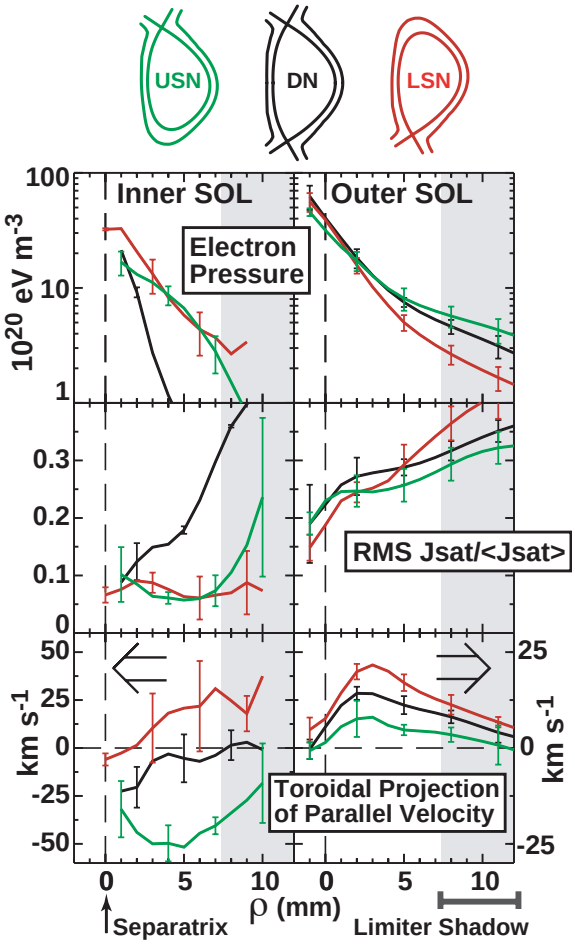

Figure 2. Scrape-off layer profile and flow data obtained from the inner and outer scanning probes. The flux surface coordinate, ρ, is the distance into the SOL, mapped to the outer midplane. Shaded regions indicate where field lines may contact limiter surfaces. Positive velocities correspond to flow in the co-current direction.

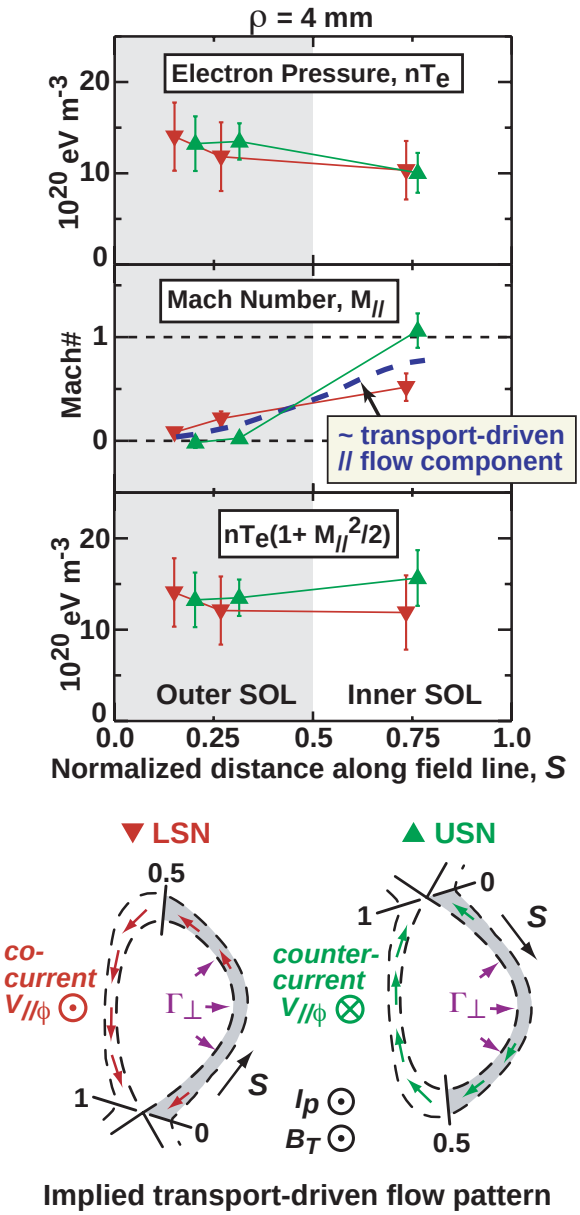

Figure 3. Probe data mapped onto a flux tube coordinate system (top panels) and implied transport-driven plasma flow pattern (bottom). Straight lines connecting between symbols are included to guide the eye. Positive Mach number corresponds to flow in the direction of *S*.

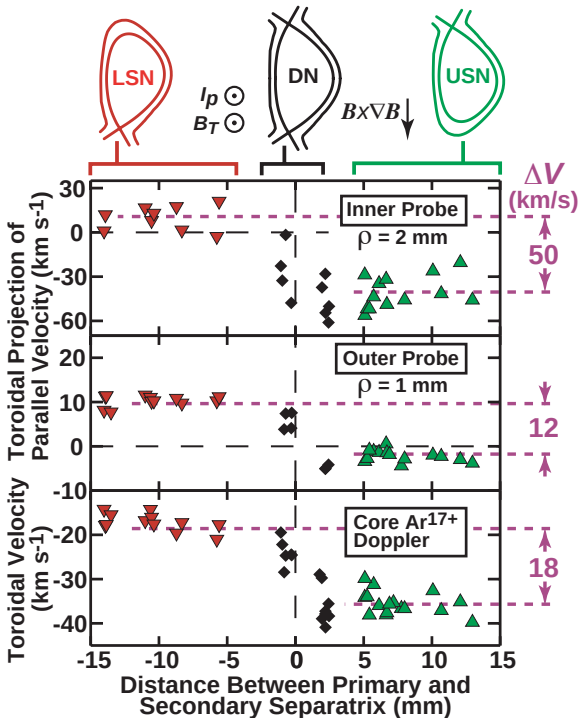

Figure 4. Toroidal projection of parallel flows measured near the separatrix by probes (top two panels) and toroidal rotation velocity measured at the plasma center (bottom panel). Positive velocity is in the direction of plasma current. The distance between primary and secondary separatrix surfaces (mapped to the outer midplane) is used to parameterize the upper/lower x-point balance.

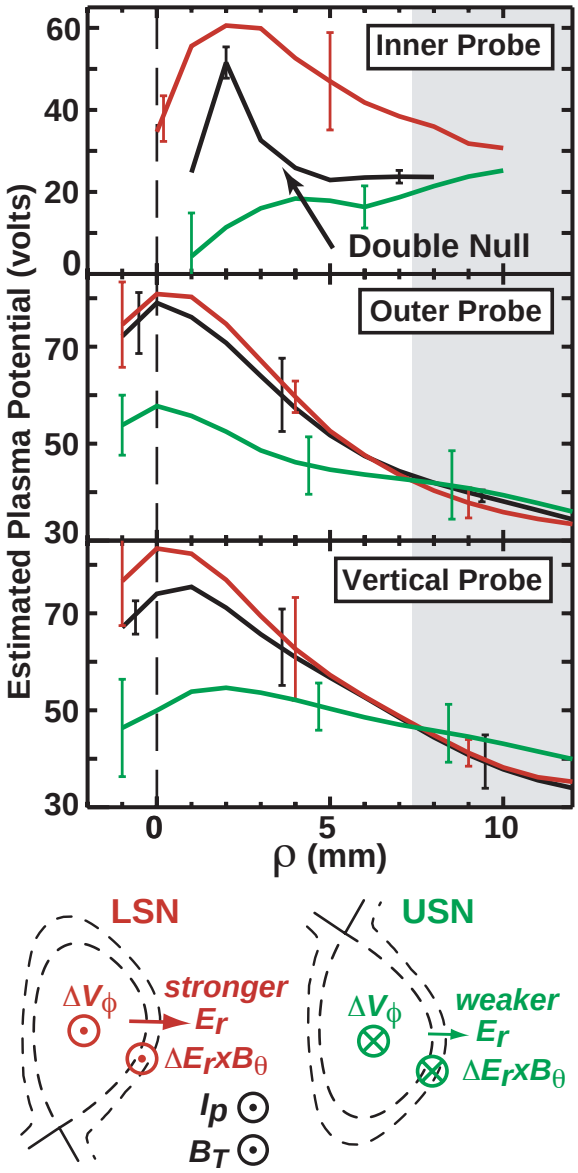

Figure 5. Plasma potential profiles in LSN/DN/USN discharges estimated from scanning probes (top panels) and the expected changes in SOL radial electric fields (bottom).

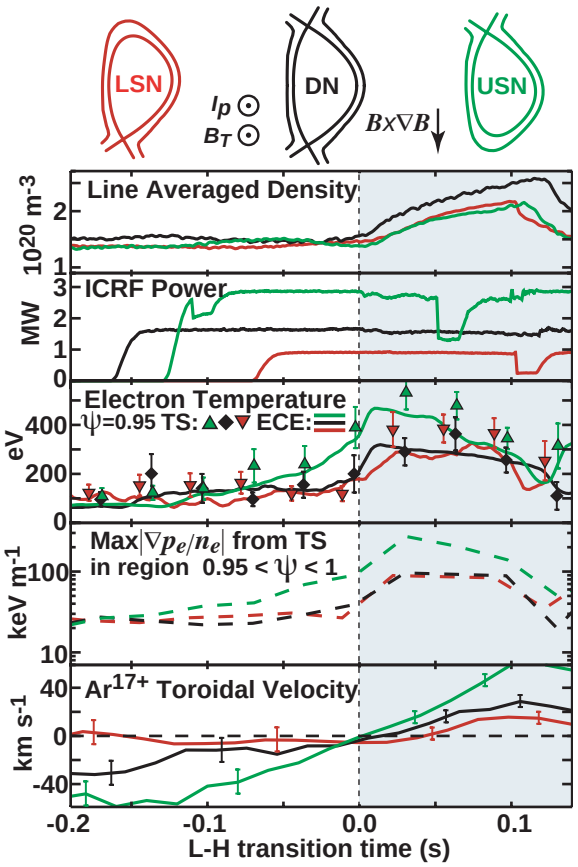

Figure 6. Time histories of thee discharges exhibiting L-H transitions near power threshold. The time axis is offset, placing zero at the time of L-H transition. Positive velocity corresponds to toroidal rotation in the co-current direction (bottom panel).

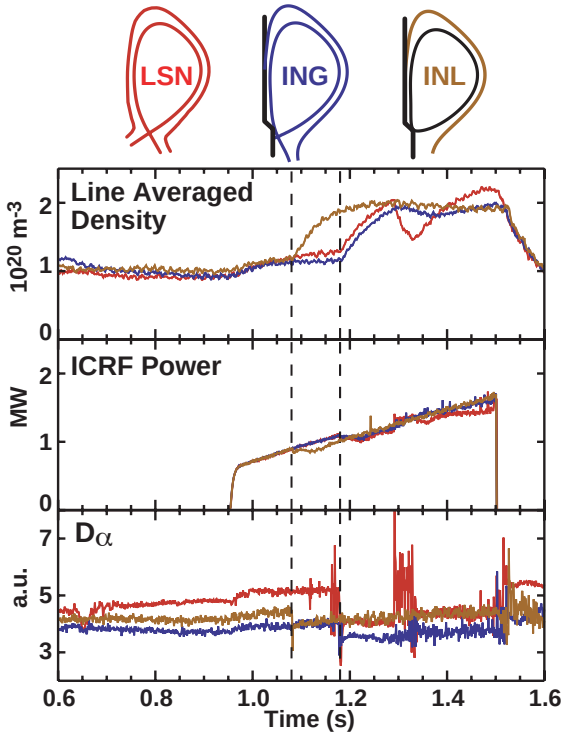

Figure 7. Time histories of LSN, ING and INL discharges exhibiting L-H transitions. Dashed lines indicate times of L-H transitions.

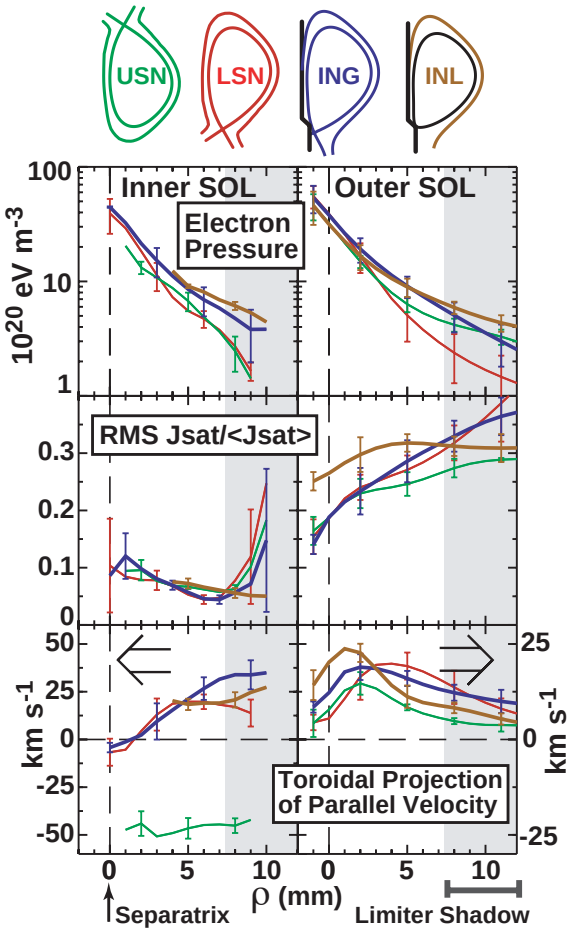

Figure 8. SOL profiles for USN, LSN, ING and INL configurations. Shaded regions indicate where field lines may connect to limiter surfaces other than the inner divertor 'nose'. Positive velocities correspond to flow in the co-current direction.

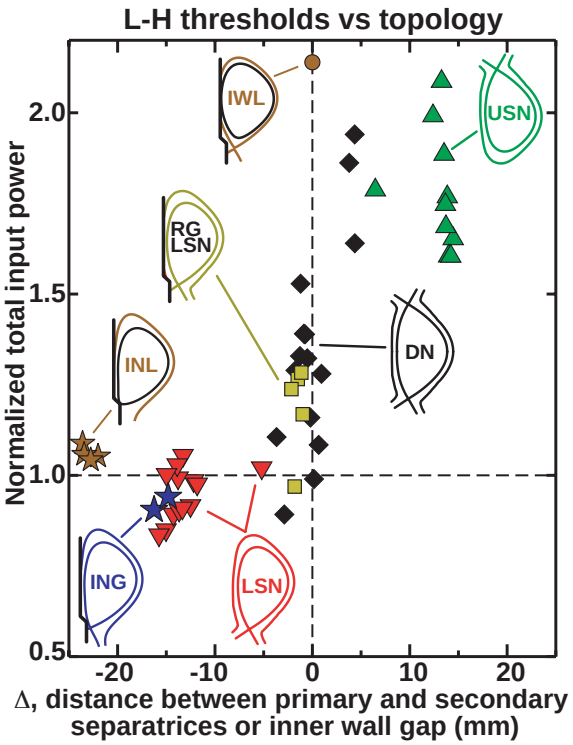

Figure 9. L-H power thresholds observed for 7 different x-point and limiter-defined magnetic configurations, normalized by a scaling law for LSN power thresholds [Eq. (1)]. The parameter, Δ, corresponds to the smaller of (i) the distance between primary and secondary separatrix surfaces (mapped to outer midplane) or (ii) the distance from the LCFS to the inner wall midplane, multiplied by minus one when a lower x-point or a lower limiter surface defines the LCFS.